On-chip Generation of Structured Light Based on Metasurface Optoelectronic Integration

Qiu-hua Wang, Pei-nan Ni, Yi-Yang Xie, Qiang Kan, Pei-pei Chen, Pan Fu, Jun Deng, Tai-lai Jin, Hong-da Chen, Ho Wai Howard Lee, et al.

On-chip Generation of Structured Light Based on Metasurface Optoelectronic Integration

Qiu-Hua Wang, Pei-Nan Ni, Yi-Yang Xie*, Qiang Kan, Pei-Pei Chen, Pan Fu, Jun Deng, Tai-Lai Jin, Hong-Da Chen, Ho Wai Howard Lee, Chen Xu*, and Patrice Genevet**

Q. H. Wang, Prof. Y. Y. Xie, P. Fu, J. Deng, T. L. Jin, Prof. C. Xu
Key Laboratory of Optoelectronics Technology
Ministry of Education
Beijing University of Technology
Beijing, 100124, China
E-mail: xieyiyang@bjut.edu.cn, xuchen58@bjut.edu.cn

Dr. P. N. Ni, Dr. P. Genevet
Université Côte d'Azur
Centre de Recherche sur l'Hétéro-Epitaxie et ses Applications (CRHEA)
CNRS
Valbonne, 06560, France
E-mail: patrice.genevet@crhea.cnrs.fr

Dr. P. N. Ni, Prof. H. W. H. Lee
Department of Physics
Baylor University
Waco, TX 76798, United States
E-mail: peinan_ni@baylor.edu

Prof. Q. Kan, Prof. H. D. Chen
Institute of Semiconductor
Chinese Academy of Sciences
Beijing, 100083, China

Prof. P. P. Chen
National Centre for Nanoscience and Technology
Beijing, 100190, China

Prof. H. W. H. Lee
Department of Physics & Astronomy
University of California
Irvine, CA 92697, United States

Keywords: Metasurface, Structured light, VCSELs, Semiconductor lasers, Optoelectronic integrations

Abstract:

Metasurfaces offer complete control of optical wavefront at the subwavelength scale, advancing a new class of artificial planar optics, including lenses, wave plates, and holograms, with unprecedented merits over conventional optical components. In particular, the ultrathin, flat and compact characteristics of metasurfaces facilitates their integration with semiconductor devices for the development of miniaturized and multifunctional optoelectronic systems. In this work, generation of structured light is implemented at an ultracompact wafer-level through the monolithic integration of metasurface with standard vertical cavity surface-emitting lasers (VCSELs). This work opens new perspectives for the design of structured light systems with compactness, lightweight, and scalability. Ultracompact beam structured laser chips with versatile functionalities are experimentally demonstrated, including multi-channel beams array generation, on-chip large angle beam steering up to 60^{o}, and wafer-level holographic beam shaping with a wide field of view (about 124^{o}). The results will promote the development of compact light structuring systems with great potential in 3D imaging, displays, robotic vision, human-computer interaction, and augmented/virtual reality.

Modern electronic devices have been reshaped with portable, affordable, and versatile functional characteristics by the rapid advancement of digital integrated circuits, computer and internet technologies. In this regard, exotic optical and photonic components are widely integrated into the electronic systems to further boost their capacities and functionalities, finding the way into a broad range of applications from instrumentation and consumer electronics to quantum information processing and communications.[1] However, conventional refractive optical elements, which rely on the accumulated phase during light propagation through media, are bulky and heavy, and their integration requires a precise alignment process, hindering the wide implementation of miniaturized systems. As an alternative, diffractive optical elements (DOEs), such as Dammann gratings and Fresnel lenses, stand out because of their significantly reduced thickness (comparable to the wavelength of light) and are thus suitable for compact on-chip optoelectronic integrations.[2, 3] However, the performance of DOEs for broad angle applications is limited by the large grating period, for instance, the deflection angles are constrained within ~ 8^{o} at a wavelength 550 nm for a grating period of 3.2 μm.[4, 5] Despite the progress of current nanofabrication techniques that allows for manufacturing blazed gratings with subwavelength scale period, DOEs are still suffering from an efficiency drop at larger deflection angles due to the light-shadowing effect[6, 7], which prevents them from wide field applications.

Artificial optical surfaces, namely metasurfaces, considered as the two-dimensional (2D) equivalence of 3D metamaterials, hold great potential to overcome current limitations of DOEs, offering the advantages of subwavelength spatial resolution, larger operation angles and higher conversion efficiency [8-11]. This new type of ultrathin flat optical component has been leveraged into a large variety of applications, including high numerical aperture lenses[12], waveplates[13], beam deflectors[14], polarization converters[15, 16], and holograms[17, 18]. Nevertheless, there are several difficulties to the wide use of current metasurfaces,

including correcting chromatic aberrations, scaling up the production of large-scale components, and extending the operation bandwidth, *etc*. To solve these problems, significant progress has been made by implementing new manufacturing techniques[19], advanced optimization and design methodologies[20-23]. Although metasurfaces are mainly demonstrated for standalone applications as individual components, it is worth stressing that their unique characteristics, including the planar configuration, negligible thickness, and compatibility with standard semiconductor fabrication techniques make them ideal for on-chip optoelectronic integrations**.** In particular**,** integrating metasurfaces with monochromatic semiconductor lasers within a well-defined emitting area opens up a feasible solution to advance ultra-compact laser systems with arbitrary beam profile controllability, which spares the realistic applications of metasurface from confronting the challenging issues of dispersion, bandwidth, and large area fabrication.[24-26]

Spatially structured light, in which the wavefront, amplitude and/or polarization are tailored to produce complex patterns and specific intensity distribution, is attracting considerable interest with its potential applications in astronomy, communication, machine vision, 3D manufacturing, stereoscopic scanning and imaging.[27-29] Despite the fact that a large variety of approaches, *i.e.* using cylindrical lens pairs, Q-plate, spiral phase plate, spatial light modulator, and Sagnac interferometers, have been utilized to generate structured light[27, 30], major difficulties, both fundamental and technological, including poor resolution, low damage threshold, and downsizing problems, remain in the way of integrating structured light source into photonics and optoelectronics applications.[31] With respect to the conventional light structuring systems, metasurfaces have proved advantages in replacement of bulky optics to shape the free space light into structured beam in a compact manner.[32] Here, we present an ultracompact solution to combat the longstanding requirement of on-chip beam structuring source via monolithic integration of dielectric metasurfaces with vertical cavity surface-

emitting lasers (VCSELs). As a proof of concept, we experimentally demonstrate compact laser structuring chips with versatile functionalities of beams array generation, on-chip large angle beam steering, and wafer-level holographic beam shaping. The characteristics of VCSELs, such as small threshold current, circular beam profile, high modulation speed, and large-scale two-dimensional array, make them highly preferred for integrated electronic and photonic applications.[33, 34] The combination of designer planar optics with VCSELs features the wafer-level generation of structured light with ultra-compactness, easy integration, and design flexibility, promising their applications in 3D imaging, directional displays, robotic vision, eye tracking, facial anthropometry, and human-computer interaction.

Design and fabrication of on-chip beam structuring devices

Figure 1a depicts the design of a metasurface integrated vertical cavity surface-emitting laser (MS-VCSEL) for on-chip generation of spatially structured beam. To facilitate the integration of the metasurface, the VCSEL is designed and fabricated into a back-emitting configuration, which employs the back side of the substrate as the emitting surface (See Supplementary Note 1 for fabrication details). Our VCSELs exhibit single fundament mode emission with the lasing wavelength of around 976 nm under the injection current of 1 mA due to the tightly confined oxide aperture (~3 μm in diameter) (Figure S1a, Supporting Information). Dielectric metasurfaces are fabricated by directly sculpturing the back surface of the GaAs wafer substrate into a nanopillars array with varying radius, as illustrated in **Figure 1b**. It is worth noticing that despite their indispensable role as material template in the state-of-the-art epitaxy of semiconductor thin films, use of wafer substrates typically causes several problems including low light extraction efficiency, poor thermal and electrical conductivity, limiting the performance of semiconductor optoelectronic devices, such as LEDs and lasers. To solve those issues, various approaches have been developed for substrate thinning and removal, which come at the expense of increasing the fabrication complexity and introducing surface

damage. Alternatively, benefitting from the planar configuration of the metasurface, our MS-VCSELs can recycle the GaAs substrate in a favourable way by turnning it into the beam structuing metasurface, taking advantage of its high transmission coefficient and large refractive index. (See Supplementary Note 2) Moreover, since this approach simplifies the assembling process of optical components, which is generally required for 3D sensing and LiDAR applications that until now rely on heavy and bulky optical components such as micro-lenses and other complex diffraction gratings, such optoelectronic integration of metasurface offers a feasible solution for lightweight and compact structured light dots projector.

For this purpose, centro-symmetric nanopillars are chosen as the meta-atom elements, functioning as truncated waveguides, in which the effective refractive index of their optical propagating modes are determined by the pillar radii, allowing for polarization insensitive control of phase profile.[35, 36] The transmission efficiency and the phase retardation of light scattered from GaAs nanopillars (500 nm tall) are numerically analysed using finite difference time domain (FDTD) simulations as a function of the nanopillars' radius in the wavelength range from 970 nm to 990 nm (Figure S2, Supporting Information). It can be seen that GaAs nanopillars exhibit both high transmission efficiency and a full phase coverage ([0, 2π]) within this wavelength region, allowing for high efficient beam reconstruction applications. To build discretized metasurfaces that are able to satisfy the Maréchal's criterion when the performance of the metasurface is limited only by the diffraction of the light[35], we employed four equally spaced phase delaying nanopillars with four different radiuses of 56, 82, 98 and 116 nm (Figure S3, Supporting Information). The whole metasurface (200 μm in diameter) is monolithically integrated with the VCSEL by assembling the nanopillars in a subwavelength lattice constant of 260 nm by 260 nm for on-chip generation of structured beams. Note that the size of the integrated metasurfaces is set much larger than the incident laser beam (~86

μm in diameter), to maximize the coupling between the laser beam and the metasurfaces and to avoid the diffraction of light caused by the metasurface's physical boundary.

Multi-channel beams array generators

The 2D configuration of the MS-VCSELs makes them particularly suitable for the implementation of multi-channel structured light sources with programmable emissions. As a proof of concept, three different beams array generators, which divide a single laser beam into a given number of output beams with equal intensity distribution, respectively, are demonstrated on a MS-VCSELs chip. To this end, the phase profile of each metasurface is encoded into two functions, $\phi_{total} = \phi_{collimator} + \phi_{multibeams}$, where $\phi_{collimator}$ will impose a hyperboloidal distribution of phase delay at the metasurface to compensate the spherical wavefront of the incident laser beam after the oxide aperture for collimation, while $\phi_{multibeams}$ will further split the beam into an array of designer beams at given deflection angles. The design principle and the mathematic expression of the phase distribution are discussed in detail in Figure S4 (Supporting Information). The collimating phase component ($\phi_{collimator}$) plays a critical role as it helps to significantly reduce the divergence angle of the VCSEL lasers.[24] As an example, MS-VCSELs beam array generators are designed with three different phase profiles ($\phi_{multibeams}$), splitting the emitting laser beam into 1×3, 3×1, and 3×3 output beams arrays, respectively, offering an ultracompact solution for multi-channel structured light sources.

Figure 2a shows the experimental setup for the emission profile characterization of the MS-VCSEL beams array generators. The MS-VCSEL chip is mounted on a metallic heat sink and placed on a 3D rotation stage to guarantee the emitting surface is well aligned with respect to the CCD camera during the measurement. A continuous wave (*cw*) current source is used to power the laser. A CCD camera equipped with a microscope objective is fixed on a motorized stage to record the beam profiles of the laser in the three directions. **Figure 2b** shows the

intensity distribution of the generated beams array along the propagation direction (*Z*-direction). The figure summarizes the far-field intensity distributions of three devices, in which metasurfaces are designed to split the emitting beam along *X*-axis, *Y*-axis, and into *XY* plane, respectively. Accordingly, a well-collimated beams array with different controlled number of spots are observed. The efficiency of the beams array generator, which is defined as the fraction of the total incident beam power converted into the power of the output beams, summing the contributions of all beams, have been experimentally determined to be about 38.7%, 31.6%, and 26.1%, respectively. The far-field emission pattern of the multi-beams array, characterized at the distance of Z = 5cm, shows that the generated beams on the same array exhibit symmetric beam profile with comparable profiles and amplitudes (**Figure 2c**), which is further confirmed by the intensity distribution measurement of the beam array (Figure S5, Supporting Information). Moreover, the array uniformity (denoted as $\triangle R$), representing the emission power deviation of each beam from the averaged power, is measured to be 10.5%, 9.4%, and 10.7% for the 1×3, 3×1, and 3×3 arrays, respectively.

It is noteworthy that the capability of metasurfaces to tailor the phase response with subwavelength precision provide more degrees of freedom in the design of the structured light over those using conventional diffractive optical elements (DOEs), such as Dammann and kinoform gratings. For instance, the birefringence of metasurfaces can control the polarization states of light in unique manners,[15, 37] while even simpler isotropic nanopillar design could provide higher diffraction efficiency in different order and higher performance at large deflection angles than the DOEs[38], which is highly desired for wide field applications of structured light. In addition, the high refractive index dielectric metasurfaces are more suitable for harsh environment applications and easier for optoelectronic integrations than the polymer based DOEs.

Large-angle beam steering on a chip

It is noteworthy that the design of on-chip 2D array MS-VCSELs allows for individually and selectively operation of structured beam pixels, thus such optoelectronic integration of metasurfaces unlocks the potential to develop a new type of ultra-compact programmable beam steering and 3D sensing chip. To demonstrate a large-angle beam steering chip, MS-VCSELs with varying emitting angles ranging from 0^o to 60^o are fabricated into an 8 × 8 lasers array (**Figure 3**). Each metasurface on the chip is designed with a different phase profile, $\phi_{total} = \phi_{collimator} + \phi_{deflector}$, where the phase component ($\phi_{collimator}$) is imposed to collimate the incident beam and the phase $\phi_{deflector} = 2\pi - \frac{2\pi}{\lambda} x.\sin\theta$ will further deflect the beam at the given deflecting angle (θ) along the transverse direction (we choose this to be *X*-direction). **Figure 3b** shows optical images of the far-field beam patterns projected onto a screen from the same beam steering chip under the *cw* injection current of 5 mA, where intense laser spots with different deflection angles can be observed. The large-angle beam steering function is further demonstrated from this chip by programming the operation of the individual laser element, scanning the emitting beam for 0^o to 60^o (**Figure 3c**). The compactness of the fabricated beam steering chip is visualized in **Figure 3d**. The deflection efficiency of the beam steering chip is experimentally determined in the range of 47% to 71.3%, without significantly dropping when the deflection angle increases (Figure S6, Supporting Information).

Considering that in this example we have discretized the metasurface phase profile using four meta-elements, associated to four phase levels (0, π/2, π, 3π/2) with a fixed subwavelength lattice constant of 260 nm, the maximum achievable phase gradient is about 69°, according to the expression:

$$\sin(\theta_t)\, n_t - \sin(\theta_i)\, n_i = \frac{\lambda_o}{2\pi}\frac{d\emptyset}{dx}$$

where n_i and n_t are the GaAs substrate (n_i =3.52) and free space refractive indices (n_t = 1), respectively. θ_i is the incident angle, θ_t is the refraction angle, and $\frac{d\emptyset}{dx}$ is the phase gradient along *x*. Note that the proposed large angle beam steering chip contains no moving parts, which is beneficial for high speed applications. Moreover, the large beam deflection angle of the MS-VCSELs can be readily applied for the generation of wide field spatially structured light.

Wafer-level holographic beam structuring with wide field of view

The potential of the proposed beam structuring chip to produce complex wavefronts can be further revealed by implementing compact holographic display on a chip. Computer-generated holography (CGH), which has been widely employed to create 3D displays, provides a powerful tool for arbitrary wavefront reconstruction, suitable for the manipulation of phase, amplitude, and polarization. However, conventional CGH suffers from several drawbacks, such as large pixel size, small field of view, narrow space-bandwidth, and unwanted diffraction orders. As a promising alternative, metasurface based holographic techniques have demonstrated superior performance due to their subwavelength spatial resolution and ultrathin thickness.[39] In particular, the planar configuration and subwavelength thickness of metasurface holograms have great advantages to be easily integrated with optoelectronic systems for complex beam construction applications. **Figure 4a** illustrates the schematic of a wafer-level metasurface holographic beam structuring device. For this purpose, metasurface holograms, which can be encoded with arbitrary complex beam patterns through the CGH method, are integrated with the VCSELs. In this example, a phase-only CGH with lattice size of 260 nm is designed using the classical Gerchberg-Saxton algorithm to construct an image of university logo in the far field.[40] Additionally, a collimating lens phase profile ($\phi_{collimator}$) is superimposed together with the CGH phase to

compensate the diffraction in the substrate, considering that the incoming Gaussian beam upon the metasurface has a spherical wavefront.

The measured power–current–voltage (*P–I–V*) characteristics of the metasurface holographic beam structuring device confirm comparable output power and electrical properties with respect to bare VCSELs, indicating that the metasurface integration did not deteriorate the laser performance (**Figure 4b**, Figure S1c, Supporting Information). **Figure 4c and 4d** shows the far-field emission patterns projected onto a screen placed at Z = 2 cm, under the injection currents of 0.5, 1.0, 3.0 and 5.0 mA, respectively. Holographic images, free of the zeroth order laser (mostly due to the fact that the incoming wave is diverging), are constructed under different injection currents. The intensity of the holographic image increases significantly with the injection current and the more features can be resolved under higher current. Since the zeroth order laser beam is highly divergent, and thus has low amplitude, it will barely interfere with the holographic image, which is beneficial for a simple design and a high signal to noise ratio. In addition, the designed subwavelength lattice constant of the integrated metasurface hologram (p = 260 nm) considering the refractive index of the substrate (~3.5) allows for high conversion efficiency by suppressing higher diffraction orders. This can be further confirmed by the hight efficiency of the holographic image shown in Fig. 4c, which is defined as the ratio of the emission power of the image to the total laser power, and experimentally determined to be 65.7%, 65.9%, 66.0% and 66.4%, under the injection current of 0.5, 1.0, 3.0 and 5.0 mA, respectively (see Supplementary Note 3 for details). Moreover, such a subwavelength lattice constant of the metasurface holography leads to a larger field of view (FOV) than the conventional hologram which can be calculated (~124^{o}) by the expression:[41]

$$\alpha = 2\arctan(\frac{\lambda}{2p})$$

where p is the lattice period of the metasurface hologram. Therefore, the monolithic integration of a holographic metasurface with the VCSEL offers a new solution to engineer the laser beam with arbitrary phase, amplitude, and polarization profiles for wide field applications.

On the other hand, note that the dimensions of previously reported metasurface holograms are usually constrained in the range of hundreds of microns due to the difficulties in large-scale nano-fabrication, which greatly limits the spatial resolution to construct large-scale images. In addition, the reconstruction of those metasurface holographic images always relies on a bulky and expensive external laser source, conventional lens to focus the incident beam onto the metasurface hologram, and precise alignment, which inevitably increases the complexity and the size of the system. In contrast, the metasurface holographic beam structuring device proposed in this work represents a new type of integrated, ultracompact, and portable holography system with a built-in light source, offering a numerous of unique advantages. Firstly, with respect to the conventional external integration of hologram, our monolithic approach not only reduce the insertion loss of introducing optic elements into the system but also take the advantage of high fabrication precision of the nano-fabrication process with much less alignment error. Secondly, the holographic metasurface in this work is directly fabricated into the epitaxy-grade substrate material with ultra-high crystalline quality, of which the lossless nature ensures the high transmission of the output power. Thirdly, since our holographic metasurface is integrated only at the laser emitting surface, which is enough far away from the laser cavity, it doesn't change the cavity structure nor couple with the DBR mirrors. Therefore, such an integration solution is highly compatible with the fabrication process and structural configuration of the standard VCSELs, which is the most important factor that ensures our beam structuring device will exhibit comparable performance including output and electrical properties with the bare laser. Moreover, the unique 2D array

of the MS-VCSELs makes it suitable for scaling up the holographic display by stitching the high-resolution images created by different individual laser pixels. Therefore, the metasurface holographic VCSELs could greatly promote the advancement of ultracompact, lightweight, large-scale, holographic systems, which are suitable for wide field applications.

In summary, an ultracompact system for on-chip generation of structured beams with arbitrarily engineered phase profile is demonstrated by integrating phase-controlling dielectric metasurfaces with VCSELs. This work unlocks the potential of the monolithic integration of metasurface to produce complex, multibeam, and multichannel structured light source at an ultracompact level, and reveals its capability for large-angle operation by taking the advantage of the subwavelength spatial resolution of metasurface. As a proof of concept, beam structuring chips with various functionalities are experimentally demonstrated, including multi-channel beams array generation, large-angle beam steering up to 60^{o} and wafer-level holographic beam shaping with wide field of view (~124^{o}). Such a system judiciously combines the latest ultrathin flat optics techniques with the state-of-art 2D array of VCSELs, opening an entirely new perspective for the design and implementation of on-chip generation of structured beams with compactness, lightweight, large viewing angle and scalability. Moreover, we envision that the functionalities of the proposed beam structuring device can be further enriched to a greater extent by employing other types of metasurfaces, taking advantages of the fast-growing metasurface technology. For instance, monolithic integration of polarization controlling metasurface of geometric phase or elliptical cross-sections will allow for both phase and polarion control at the same time.[42-44] The results explore the versatility of metasurface optoelectronic integrations, marking a steady step toward to their realistic and applicative applications. Our technique could promote the advancement of compact structured light sources applied into the integrated electronics and optoelectronics

systems, facilitating various emerging applications in 3D imaging, directional displays, robotic vision, eye tracking, human-computer interaction, and augmented/virtual reality.

Supporting Information

Supporting Information is available from the Wiley Online Library or from the author.

Acknowledgements

Q. H. W. and P. N. N. contribute equally to this work. We acknowledge the financial support from the National Key R&D Program of China (2018YFA0209000), National Natural Science Foundation of China (62074011, 61604007, 61874145, 61774175), and the Beijing Natural Science Foundation (4172009, 4182012). P. Ni, and P. Genevet acknowledge the financial support from European Research Council (ERC) under the European Union's Horizon 2020 research and innovation program (grant agreement FLATLIGHT No 639109). H. W. H. Lee acknowledges the financial support from the National Science Foundation (grant number: 1752295). The authors acknowledge the Nanofabrication Laboratory at National Centre for Nanoscience and Technology for sample fabrication.

Received: ((will be filled in by the editorial staff))
Revised: ((will be filled in by the editorial staff))
Published online: ((will be filled in by the editorial staff))

References

[1] D. Llewellyn, Y. Ding, I. I. Faruque, S. Paesani, D. Bacco, R. Santagati, Y.-J. Qian, Y. Li, Y.-F. Xiao, M. Huber, Nature Physics 2020, 16, 148.
[2] H. Martinsson, J. Bengtsson, M. Ghisoni, A. Larsson, IEEE Photonics Technology Letters 1999, 11, 503.
[3] M. Karlsson, F. Nikolajeff, H. Martinsson, A. Larsson, "Monolithic integration of continuous-relief diffractive structures with vertical-cavity surface-emitting lasers", presented at *IEEE 18th International Semiconductor Laser Conference*, 29 Sept.-3 Oct. 2002, 2002.
[4] D. Lin, M. Melli, E. Poliakov, P. S. Hilaire, S. Dhuey, C. Peroz, S. Cabrini, M. Brongersma, M. Klug, Scientific Reports 2017, 7, 2286.
[5] D. Lin, P. Fan, E. Hasman, M. L. Brongersma, Science 2014, 345, 298.
[6] P. Lalanne, S. Astilean, P. Chavel, E. Cambril, H. Launois, J. Opt. Soc. Am. A 1999, 16, 1143.
[7] T. Hessler, M. Rossi, R. E. Kunz, M. T. Gale, Appl. Opt. 1998, 37, 4069.
[8] A. Arbabi, Y. Horie, M. Bagheri, A. Faraon, Nature nanotechnology 2015, 10, 937.
[9] N. Yu, P. Genevet, M. A. Kats, F. Aieta, J.-P. Tetienne, F. Capasso, Z. Gaburro, science 2011, 334, 333.
[10] A. V. Kildishev, A. Boltasseva, V. M. Shalaev, Science 2013, 339.
[11] E. Khaidarov, Z. Liu, R. Paniagua-Domínguez, S. T. Ha, V. Valuckas, X. Liang, Y. Akimov, P. Bai, C. E. Png, H. V. Demir, A. I. Kuznetsov, Laser & Photonics Reviews 2020, 14, 1900235.
[12] S. Wang, P. C. Wu, V.-C. Su, Y.-C. Lai, M.-K. Chen, H. Y. Kuo, B. H. Chen, Y. H. Chen, T.-T. Huang, J.-H. Wang, Nature nanotechnology 2018, 13, 227.
[13] F. Ding, Z. Wang, S. He, V. M. Shalaev, A. V. Kildishev, ACS nano 2015, 9, 4111.
[14] L. Wang, S. Kruk, K. Koshelev, I. Kravchenko, B. Luther-Davies, Y. Kivshar, Nano letters 2018, 18, 3978.
[15] Q. Song, A. Baroni, R. Sawant, P. Ni, V. Brandli, S. Chenot, S. Vézian, B. Damilano, P. de Mierry, S. Khadir, Nature communications 2020, 11, 1.
[16] Y. Chen, J. Gao, X. Yang, Laser & Photonics Reviews 2018, 12, 1800198.
[17] H. Ren, G. Briere, X. Fang, P. Ni, R. Sawant, S. Héron, S. Chenot, S. Vézian, B. Damilano, V. Brändli, Nature communications 2019, 10, 1.
[18] L. Huang, H. Mühlenbernd, X. Li, X. Song, B. Bai, Y. Wang, T. Zentgraf, Advanced Materials 2015, 27, 6444.
[19] G. Brière, P. Ni, S. Héron, S. Chenot, S. Vézian, V. Brändli, B. Damilano, J. Y. Duboz, M. Iwanaga, P. Genevet, Advanced Optical Materials 2019, 7, 1801271.
[20] S. Molesky, Z. Lin, A. Y. Piggott, W. Jin, J. Vucković, A. W. Rodriguez, Nature Photonics 2018, 12, 659.
[21] J. Jiang, J. A. Fan, Nanophotonics 2019.
[22] M. M. Elsawy, S. Lanteri, R. Duvigneau, G. Brière, M. S. Mohamed, P. Genevet, Scientific Reports 2019, 9, 1.
[23] M. M. R. Elsawy, S. Lanteri, R. Duvigneau, J. A. Fan, P. Genevet, Laser & Photonics Reviews, n/a, 1900445.
[24] Y. Y. Xie, P. N. Ni, Q. H. Wang, Q. Kan, G. Briere, P. P. Chen, Z. Z. Zhao, A. Delga, H. R. Ren, H. D. Chen, C. Xu, P. Genevet, Nat Nanotechnol 2020, 15, 125.
[25] K. Li, Y. Rao, C. Chase, W. Yang, C. J. Chang-Hasnain, Optica 2018, 5, 10.
[26] M. S. Seghilani, M. Myara, M. Sellahi, L. Legratiet, I. Sagnes, G. Beaudoin, P. Lalanne, A. Garnache, Scientific reports 2016, 6, 38156.
[27] H. Rubinsztein-Dunlop, A. Forbes, M. V. Berry, M. R. Dennis, D. L. Andrews, M. Mansuripur, C. Denz, C. Alpmann, P. Banzer, T. Bauer, Journal of Optics 2016, 19, 013001.

[28] S. Palagi, A. G. Mark, S. Y. Reigh, K. Melde, T. Qiu, H. Zeng, C. Parmeggiani, D. Martella, A. Sanchez-Castillo, N. Kapernaum, Nature materials 2016, 15, 647.
[29] D. Scharstein, R. Szeliski, "High-accuracy stereo depth maps using structured light", presented at *2003 IEEE Computer Society Conference on Computer Vision and Pattern Recognition, 2003. Proceedings.*, 2003.
[30] A. Vijayakumar, C. Rosales-Guzmán, M. Rai, J. Rosen, O. Minin, I. Minin, A. Forbes, Optics express 2019, 27, 6459.
[31] F. Yue, D. Wen, J. Xin, B. D. Gerardot, J. Li, X. Chen, ACS photonics 2016, 3, 1558.
[32] J. Wang, Chinese Optics Letters 2018, 16, 050006.
[33] K. Hirose, Y. Liang, Y. Kurosaka, A. Watanabe, T. Sugiyama, S. Noda, Nature Photonics 2014, 8, 406.
[34] A. J. Danner, J. J. R. Jr., P. O. Leisher, K. D. Choquette, Applied Physics Letters 2006, 88, 091114.
[35] J. Engelberg, C. Zhou, N. Mazurski, J. Bar-David, A. Kristensen, U. Levy, Nanophotonics 2020, 9, 361.
[36] R. Sawant, P. Bhumkar, A. Y. Zhu, P. Ni, F. Capasso, P. Genevet, Advanced Materials 2019, 31, 1805555.
[37] S. Banerji, M. Meem, A. Majumder, F. G. Vasquez, B. Sensale-Rodriguez, R. Menon, Optica 2019, 6, 805.
[38] D. Lin, M. Melli, E. Poliakov, P. S. Hilaire, S. Dhuey, C. Peroz, S. Cabrini, M. Brongersma, M. Klug, Scientific reports 2017, 7, 1.
[39] L. Huang, S. Zhang, T. Zentgraf, Nanophotonics 2018, 7, 1169.
[40] R. W. Gerchberg, W. O. Saxton, Optik 1972, 35, 237.
[41] Y. Hu, X. Luo, Y. Chen, Q. Liu, X. Li, Y. Wang, N. Liu, H. Duan, Light: Science & Applications 2019, 8, 1.
[42] Y. He, P. Wang, C. Wang, J. Liu, H. Ye, X. Zhou, Y. Li, S. Chen, X. Zhang, D. Fan, ACS Photonics 2020, 7, 135.
[43] Y. He, Y. Li, J. Liu, X. Zhang, Y. Cai, Y. Chen, S. Chen, D. Fan, Scientific Reports 2017, 7, 6814.
[44] F. Ding, B. Chang, Q. Wei, L. Huang, X. Guan, S. I. Bozhevolnyi, Laser & Photonics Reviews 2020, 14, 2000116.

Figures：

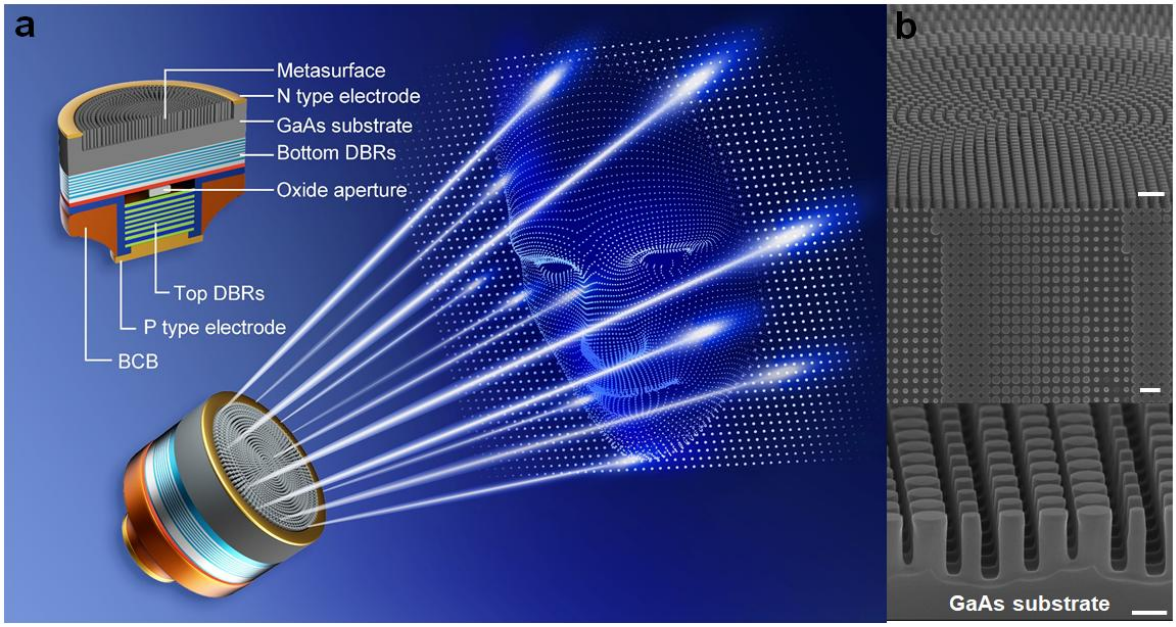

Figure 1. On-chip generation of structured beams. a) Schematic of a MS-VCSEL for ultracompact generating structured light on a chip, in this example, 2D near-infrared beam array is densely created and projected on to an object for 3D facial anthropometry. The inset illustrates the structural details of the proposed device, in which the beam structuring metasurface is monolithically integrated at the substrate back surface of a standard back-side emitting VCSEL. b) Scanning electron micrographic images of a typical integrated metasurface in the proposed beam steering chips, which is composed of GaAs nanopillars with varying radius. Various structured beams with specific phase profiles can be constructed by assembling the nanopillars so that a given phase retardation profile is imported onto the emitting beams to both compensate the diffracting effect inside the wafer substrate and to further reshape the beams with arbitrary wavefront. The scale bars are 500 nm, 500 nm, and 200 nm, respectively.

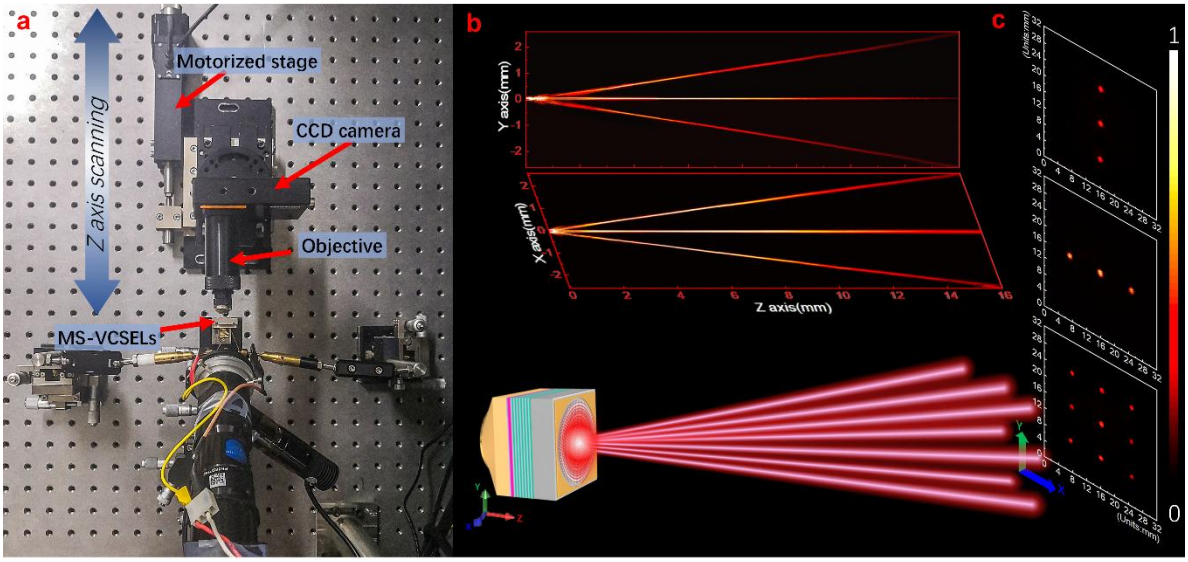

Figure 2. Multi-channel beams array generations. a) Experimental setup for the laser beam profile characterization, a CCD camera equipped with an objective (40× magnification, NA = 0.6) is mounted on a motorized stage with movement precision of 1μm to record the intensity distribution of the laser beams in three directions. b) Measured beam intensity profiles of the 3×1 (top) and 1×3 beams array (middle). The bottom is the schematic illustration of on-chip generation of 3×3 beam array. c) Measured transverse plane (*XY* plane) intensity distributions of the 3×1 (top), 1×3 (middle), and 3×3 beams array, at Z = 5 cm, respectively, revealing the generation of multi-channel beam arrays with comparable profile and amplitude.

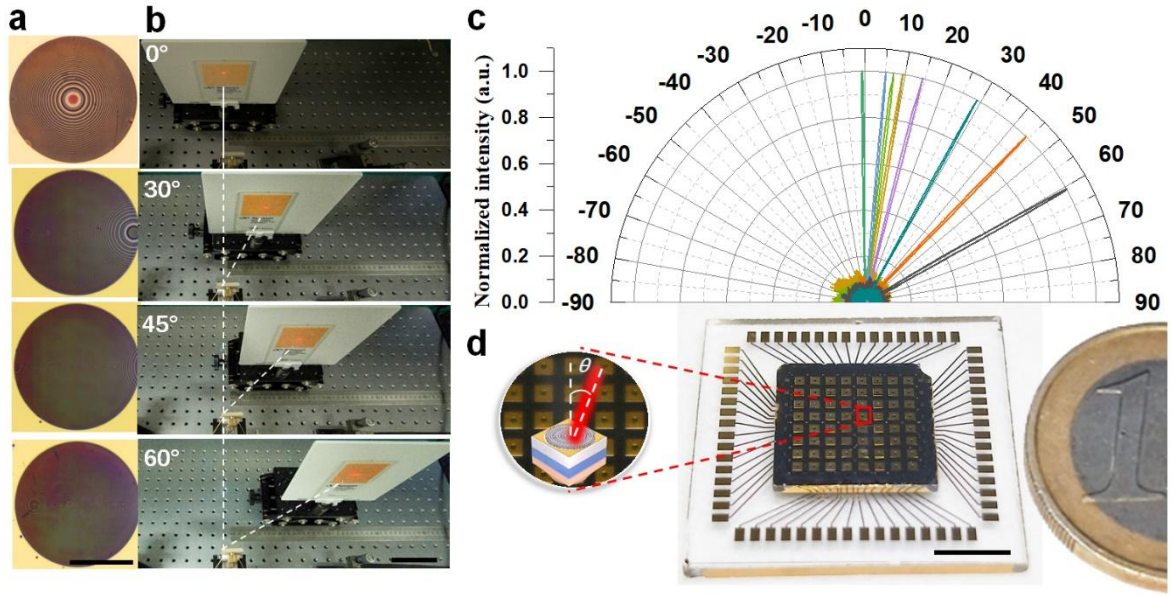

Figure 3. Large angle beam steering on a chip. a) Optical microscope images of four integrated beam deflecting metasurfaces with deflection angles ranging from 0^o to 60^o. b) Measured beam spots projected onto a far-field screen at Z = 10 cm from the same chip by selectively operating the laser element under the same injection current of 5 mA, respectively, revealing directional emission at different deflection angles. c) The polar representation of the measured emitting beams on the chip, confirming the functionality of the proposed chip as large angle beam steering. d) Optical image of the beam steering chip consisting of 8×8 laser elements with different deflection angles in the range from 0^o to 60^o, mounted onto an electric board for electrical connection. The inset shows the schematic of the individual beam deflecting laser element with a deflection angle denoted as θ. The image of one-euro coin is included for size comparison. The scale bars are 100 μm, 10 cm, and 5 mm in a), b), and d), respectively.

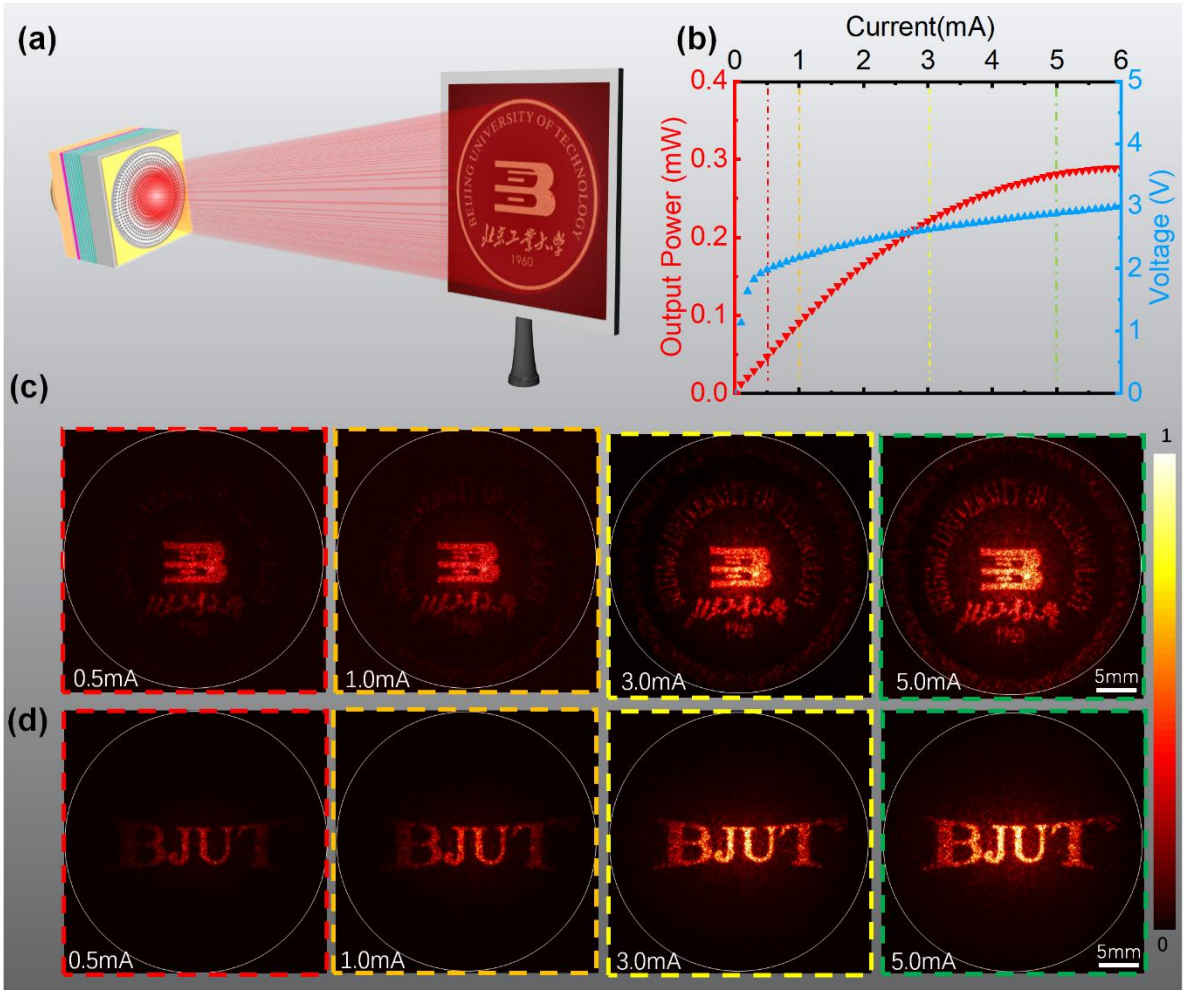

Figure 4. Wafer-level holographic beam structuring with large field of view. a) Schematic illustration of a holographic MS-VCSEL for the construction of complex beam patterns, in this example, an infrared image of university logo is constructed and directly projected onto a screen for observation. b) The *P-I-V* characteristics confirm that the holographic MS-VCSEL has comparable performance as the bare laser prior to the integration of holographic metasurface. c) and d) Experimentally reconstructed images directly from two different holographic MS-VCSELs under 0.5, 1, 3, and 5 mA, respectively, showing that the intensity of the image increases as the injection current increases and more features can be resolved at higher current. The scale bar is 5 mm.

The table of contents:

On-chip generation of structured light is demonstrated via monolithic integration of dielectric metasurfaces with standard vertical cavity surface-emitting lasers (VCSELs). This new type of ultracompact beam structuring chip exhibits versatile functionalities, including multi-channel beams array generation, on-chip large angle beam steering up to 60^{o}, and wafer-level holographic beam shaping with a wide field of view.

Keyword metasurfaces, structured light, VCSELs, semiconductor lasers, optoelectronic integrations

Qiu-Hua Wang, Pei-Nan Ni*, Yi-Yang Xie*, Qiang Kan, Pei-Pei Chen, Pan Fu, Jun Deng, Tai-Lai Jin, Hong-Da Chen, Ho Wai Howard Lee, Chen Xu*, and Patrice Genevet*

Title: On-chip Generation of Structured Light Based on Metasurface Optoelectronic Integration

ToC figure:

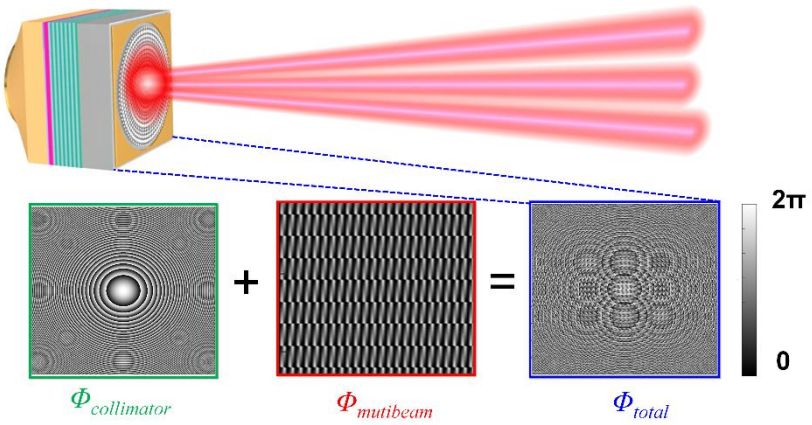

Supporting Information

On-chip Generation of Structured Light Based on Metasurface Optoelectronic Integration

Qiu-Hua Wang, Pei-Nan Ni, Yi-Yang Xie*, Qiang Kan, Pei-Pei Chen, Pan Fu, Jun Deng, Tai-Lai Jin, Hong-Da Chen, Ho Wai Howard Lee, Chen Xu*, and Patrice Genevet**

Supplementary Text:

Supplementary Note 1: Fabrication of back-side emitting VCSELs.

In order to operate the VCSELs under low injection currents without additional cooling, a large number of distributed Bragg reflectors (DBRs), 30.5 pairs of *p*-type top DBRs and 28 pairs of *n*-type bottom DBRs, which are composed of alternating $Al_{0.9}Ga_{0.1}As/Al_{0.12}Ga_{0.88}As$ layers, are utilized in the design of the laser structure. In addition, a 30 nm $Al_{0.98}Ga_{0.02}As$ oxidation layer is sandwiched between the top DBRs and the active region. The manufacturing starts by depositing a 500 nm thick SiO_2 on the top of epitaxy wafer as a hard mask by PECVD. Then, circular mesas (diameter = 50 μm, height = 5 μm) are defined by UV lithography and inductively coupled plasma reaction ion etching (ICP-RIE). The residual SiO_2 was removed by BOE etching. After that, the $Al_{0.98}Ga_{0.02}As$ layer was selectively oxidized to precisely define a small size(3μm in diameter) of current confinement aperture, which plays a critical role in ensuring the single fundamental mode operation of the laser. Then, another 500 nm thick SiO_2 passivation layer was deposited onto the top surface, followed by the planarization of the surface via spin-coating of a thick layer of Benzocyclobutene (BCB). After that, the BCB layer and the SiO_2 passivation layer on top of the mesas were selectively removed by reactive ion etching (RIE) using SF_6 as the etching gas, and by BOE chemical etching, respectively. Finally, top *P*-contacts (Ti/Au) and bottom *N*-contacts (AuGeNi/Au) were fabricated by a double-side photolithography, lift-off and a rapid thermal annealing was performed to improve the ohmic contacts.

Supplementary Note 2: Monolithic integration of metasurfaces with VCSELs.

Metasurfaces were integrated at the back surface of the substrate by directly scrupling the GaAs substrate into nanopillar structure with given dimensions. To do this, electron beam lithography (EBL) was used to define the metasurface patterns into a 180 nm thick Hydrogen silsesquioxane (HSQ) layers, which also serves as the hard mask. After that, ICP-RIE etching was used to fabricate the GaAs nanopillars with optimized conditions to minimize the surface damage. Since no etch-stop layer was introduced in the current design of the laser structure, the etching depth of the nanostructures was carefully adjusted by controlling the etching time.

Supplementary Note 3: Measurement of efficiency.

The emitting laser power is measured using a power meter (Thorlabs, Model:PM400) equipped with a silicon sensor (Thorlabs, Model:S120C). The efficiency of the holographic MS-VCSEL is defined as the ratio of the total power of constructed image to the emitting laser beam power measured at the surface of metasurface.

Supplementary Figures:

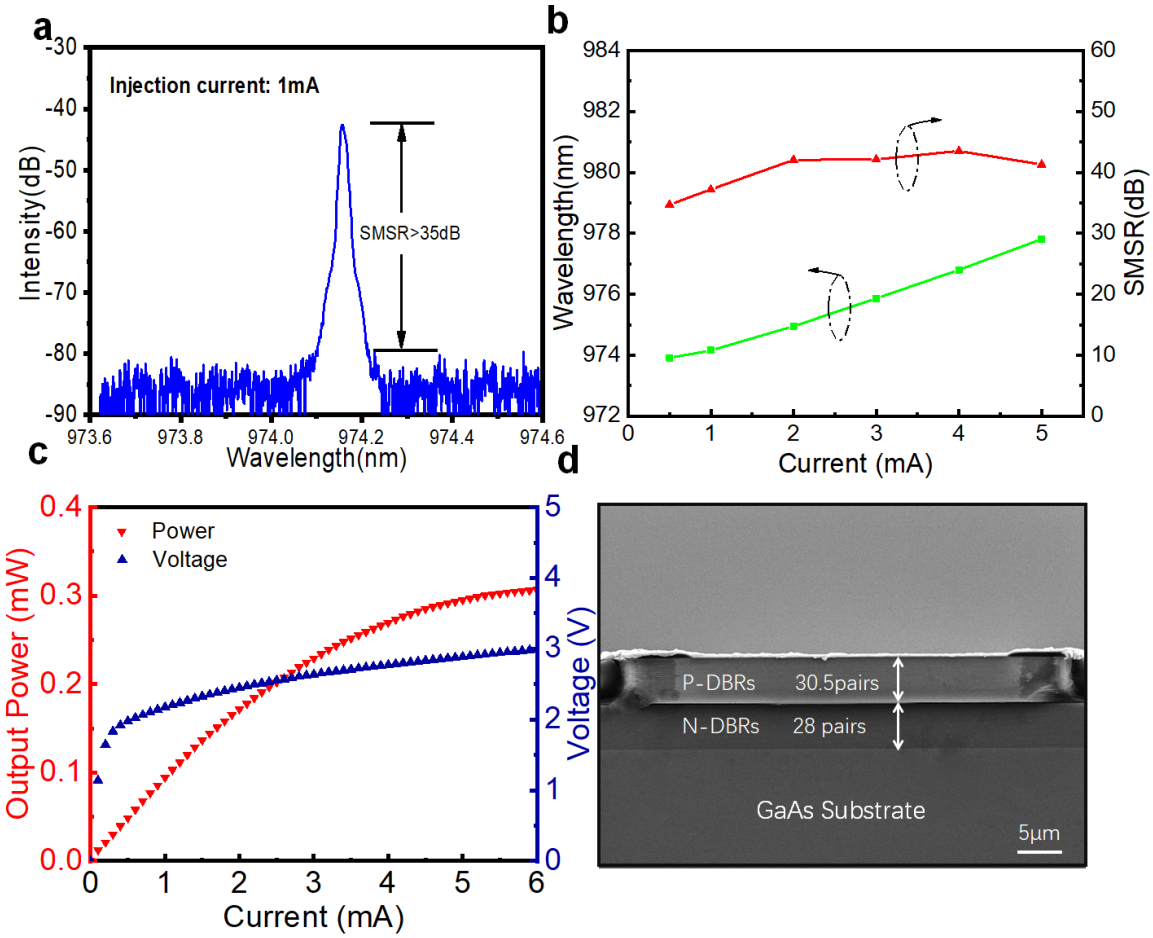

Figure S1. Lasing characteristics of the fabricated VCSELs with 3 μm oxide aperture under different injection currents. a) The emission spectra of the laser under the continuous injection current of 1mA. The single fundamental transverse mode operation of the laser is evidenced both by the FWHM of the lasing peak (less than 0.02nm) and the side mode suppression ratio (SMSR) (> 35 dB). b) shows that the lasing wavelength redshifts from about 975.7 nm to 978.9 nm when increasing the injection current from 0.5mA to 5mA since no additional cooling apparatus was employed during the measurements, while SMSR remains in the range from 40 to 50 dB. c) The *P-I-V* performances of the VCSELs prior to the integration with metasurface. Note that we employ a large number of pairs of DBRs (30.5 pairs of P-DBRs and 28 pairs of N-DBRs) in the laser design to increases the quality factor of the cavity, which results in a low threshold current (about 0.06mA), allowing for the operation of the laser

under small injection current. However, the large number of pairs of DBRs, on the other hands, limits the emission power of the laser. Therefore, the laser power of our device can be further increased by using fewer number of DBRs. d) The cross-section SEM image of the fabricate VCSEL illustrates the large number of the DBRs employed in this laser structure.

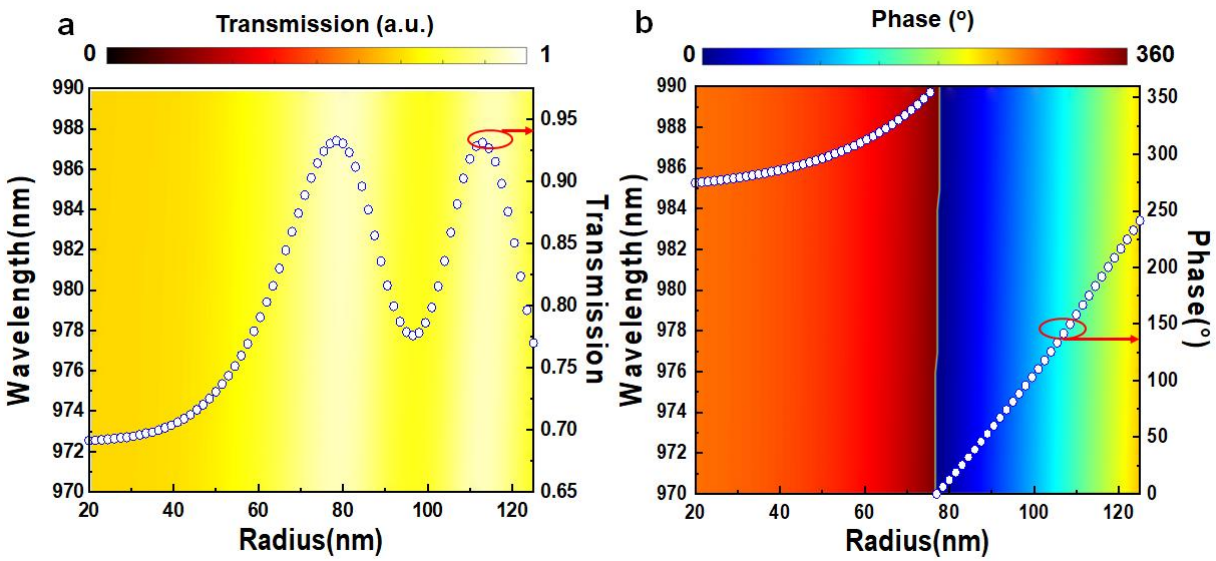

Figure S2. Calculated transmission a) and relative phase retardation b) passing through GaAs nanopillars as a function of the radius for different emission wavelength ranging from 970 nm to 990 nm. The inset curves in a) and b) show the transmission and phase calculated at the wavelength of 976 nm (corresponding to the lasing wavelength under the injection current of 1 mA), respectively. It can be seen that both the transmission and the phase retardance of the transmitted light from the nanopillars remain almost the same within this wavelength range. Considering the redshifts of the lasing under the above injection currents, it therefore ensures that the beam structuring performance of the MS-VCSELs will not be affected by the wavelength redshifts within this injecting current range.

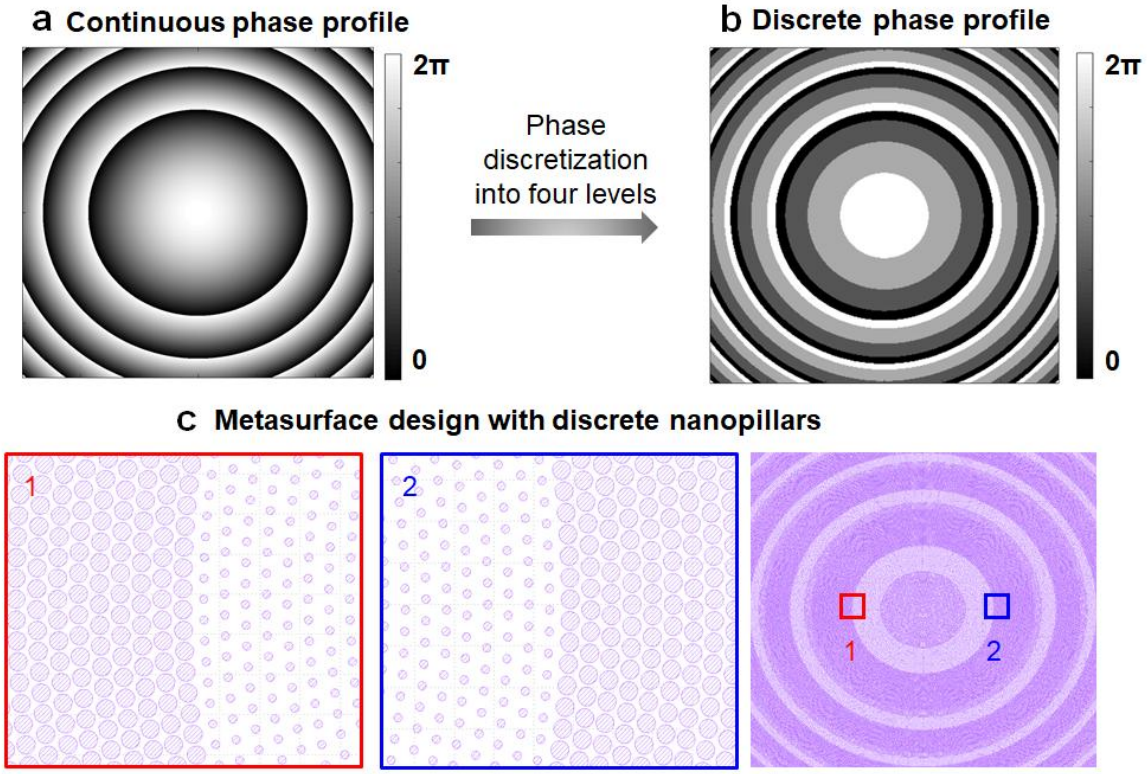

Figure S3. Phase discretization and layout of the metasurface design. a) Continuous phase pattern, this example corresponds to the phase profile of a collimator. b) Discrete phase pattern with four phase levels. c) The layout of the metasurface design assembled with nanopillars with different radius, corresponding to b). The insets show zoom-in regions of the metasurface layout.

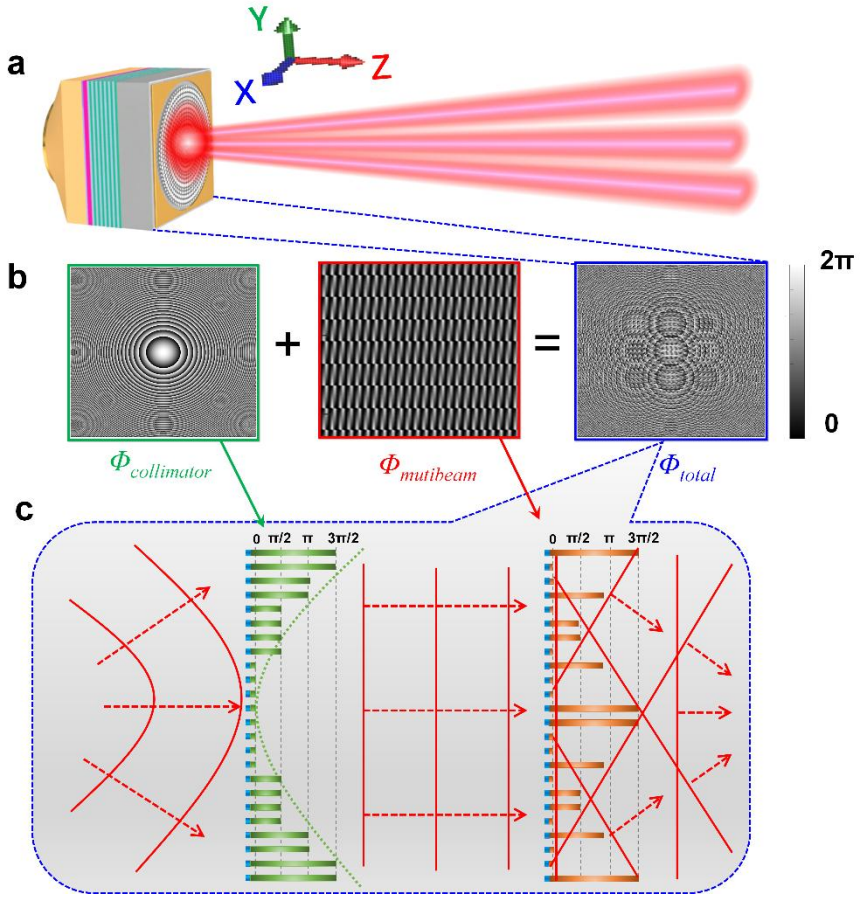

Figure S4. Phase profile design for beams array generations. a) The schematic illustration of a MS-VCSELs for the generation of 3×1 beams array. In this example, a multibeam metasurface is designed and integrated with VCSEL, which can split the emitting beam into 3×1 array in the *XY* plane. b) The phase profile of the designed metasurface multiplier in this example. The phase of the metasurface, (ϕ_{total}), is composed by superimposing the collimating phase delay($\phi_{collimator}$) with an additional phase retardation to further split and deflect the collimated wave into an assembly of tilted plane waves with different angles. Φ_{total}= $\Phi_{collimator}$+ $\Phi_{multiplier}$. Specifically, the collimating phase is determined by $\phi_{collimator}(x,y)=2\pi-\frac{2\pi n}{\lambda}(\sqrt{x^2+y^2+f^2}-f)$, where f is the focal length, n is the refractive index of the substrate. To further create a M×N beams array, the phase distribution $\Phi_{multiplier}(x,y)$ of each generated beam is denoted as $\Phi_{m,n}(x,y)$ can be determined by $\Phi_{m,n}(x,y)$ $=2\pi-\frac{2\pi}{\lambda}x\sin\theta_{xz}-\frac{2\pi}{\lambda}y\sin\theta_{yz}$, where $x=m\cdot p\cdot i$, $y=n\cdot p\cdot i$, p is the lattice period, i is

a integer, θ_{xz} and θ_{yz} represent the designed deflection angles between the *z* axis and the projections of each generated beam in the *XZ* plane and *YZ* plane, respectively. c) The schematic illustration of the function of each phase component in the design of beam array generator. The collimator phase component (Φ_{total}) will create a hyperbolic phase retardation profile to compensate the spherical wavefront of the emitting beam from the oxide aperture into plane wave out-going beam. The multiplier phase component ($\Phi_{multiplier}$) will further split the incident beam into a beam array and deflect the generated beam into given angles, respectively. The $\Phi_{multiplier}$ is determined by sampling a target complex wavefront composed of different tiled plane waves, as illustrated in the figure. In this example, the beam is divided into 3×1 beams array and deflected with -10^o, 0^o, and 10^o, along the *y* axis, respectively.

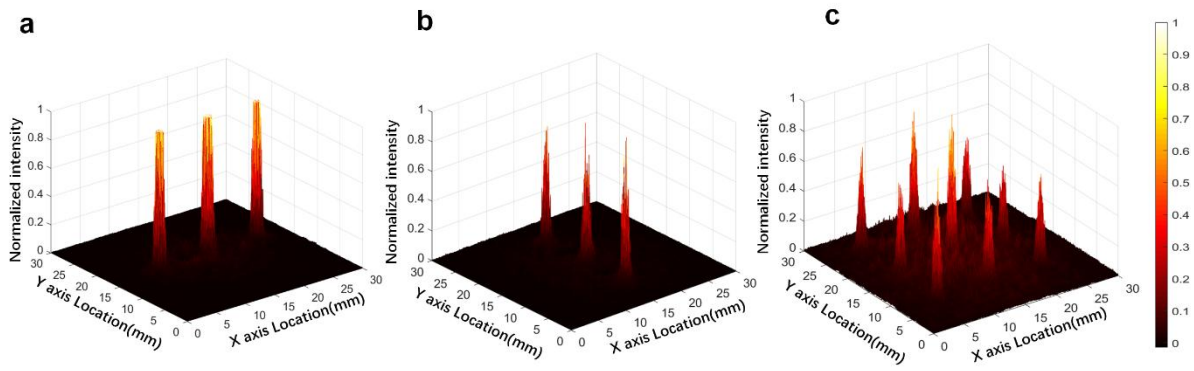

Figure S5. Intensity profiles of the generated beams arrays. The experimentally measured intensity distributions of 1×3 (a), 3×1 (b), and 3×3 (c) beams arrays show that the proposed beams array generator is enable to produce beams with similar profile and amplitude.

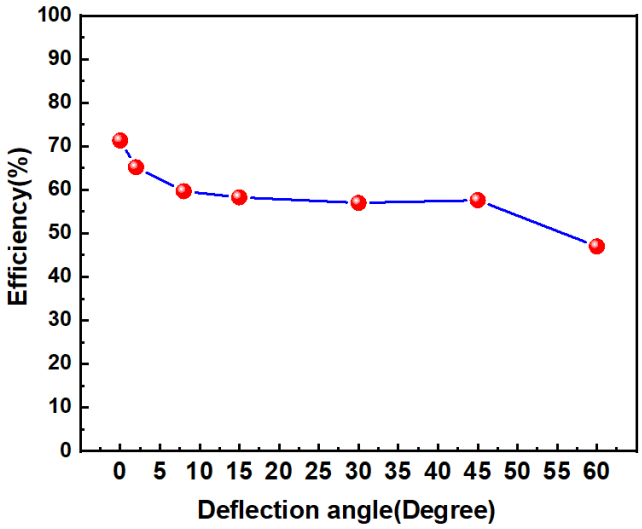

Figure S6. Beam deflection efficiency as a function of deflecting angle. The beam deflection efficiency is defined as the ratio of the power of the deflected beam measured at Z = 10 cm to the total incident beam power measured at the surface of metasurface. The experimentally measured deflection efficiency of MS-VCSELs beam steering chip indicate good beam deflection efficiency over a large range of angles without significant efficiency drop.